Trellis Coding of Two Consecutive Full Response 4-ary CPFSK with Modulation Index 1/4

Ho-kyoung Lee[1] Dariush Divsalar[2] and Charles Weber[1]

Communication Sciences Institute[1]
University of Southern California
Los Angeles, CA 90089-2565

Jet Propulsion Laboratory
California Institute of Technology
Pasadena, CA 91109

Abstract

It is well known that trellis coded modulation schemes using multidimensional constellations for PSK and QAM have a number of advantages over the more common two dimensional schemes [I], [2]. A new representation of CPM signals in multiple time slots is obtained by using parallel transitions of the trellis structure and memoryless mapping. Specific optimum outer convolutional encoders of two consecutive full response 4-CPFSK with modulation index 1/4 are achieved by application of the set partition approach. the two consecutive full response 4-ary CPFSK signals that diverge from the same state is presented. 'l'he pre-encoder design is made for the 2 to 16 states by using this set partitioning. We obtain a 5.2 to 7.5 dB power gain over the uncodcd 4-ary CPFSK full response system,

1 Introduction

Rimoldi [3], [4] showed that the generation of a continuous ***phase modulation*** (CPM) waveform can be decomposed into a time invariant ***continuous phase encoder*** (CPE) and a time invariant ***memoryless modulator*** (MM). This decomposition of CPM makes it possible to consider the CPE and the MM separately.

This paper proposes a new construction which is designated as the N-consecutive ***phase encoder*** (NCPE), and is designed to function with an MM. This construction generates an alphabet of N consecutive full response CPM signals. With a simple C} 'E, onc signal from an alphabet of 2^q signals is used to transmit q – 1 bits per time interval with a ***trellis-coded modulation*** (TCM) scheme of rate (g – I)/g. With NCPE, one signal from an alphabet of 2^{Nq} signals (which takes N time intervals) is used to transmit Nq - 1 bits every N time intervals with a TCM scheme of rate $(Nq-1)/Nq$ ***i.e.,*** NCPE makes it possible to design a higher rate binary pre-encoder. Specifically, instead of adding one redundant bit every time slot of the CPM system, one redundant bit is added every N time slots. As a special case, this paper considers a trellis encoder for two consecutive 4-ary ***continuous phase frequency shift keying*** (CPFSK) signals. In Section 3, wc present an NCPE trellis structure and corresponding memoryless modulator for the consecutive CPFSK signals. In Section 4, set ***partitioning*** of

2 Representation of CPM

CPM is a modulation scheme which carries information in the phase. We define the CPM waveform as

$$s(t,\alpha) \triangleq \sqrt{\frac{2\mathcal{E}}{T}} \cos(2\pi f_0 t + \phi(t,\alpha) + \varphi_0), \quad (1)$$

where the information-carrying phase is

$$\phi(t,\alpha) \triangleq 2\pi h \sum_{i=0}^{\infty} \alpha_i f(t-iT), \qquad t \geq 0 \quad (2)$$

$\mathcal{E}$ is the symbol energy, and the parameter h is referred to as the modulation ***index.*** Generally and practically, h is a rational number, which wc represent as

$$h \triangleq \frac{K}{P}, \quad (3)$$

where K and P arc relatively prime positive integers. The information sequence $\{\alpha_i\}$ in (2) is from an M-ary alphabet, and is given by

$$\alpha \stackrel{A}{=} (\alpha_0, \alpha_1, \alpha_2, \cdots),$$
$$\alpha_i \in \{\pm 1, \pm 3, \pm 5, \cdots, \pm(M-1)\},\ M \text{ even, i} \geq \text{O} \quad (4)$$

The phase offset φ_0 will be assumed time invariant. For the full response CPFSK case, the ***phase response*** $f(t)$ can be expressed as

$$f(t) \triangleq \begin{cases} 0, & t \leq 0 \\ t/2T, & 0 < t \leq T \\ 1/2, & t > T. \end{cases} \quad (5)$$

Phases that differ by an integer multiple of 27r are, of course, physically indistinguishable.

To enhance understanding of CPM and have the same set of candidate states (see below) for every symbol time (nT), Rimoldi [3] introduced and defined a *tilted phase version* of CPM as:

$$s(t,\alpha) \triangleq \sqrt{\frac{2\mathcal{E}}{T}} \cos(2\pi f_1 t + \Psi(t,\alpha) + \varphi_0), \qquad (6)$$

where

$$\Psi(t,\alpha) \triangleq \phi(t,\alpha) + \pi h(M-1)t/T \qquad (7)$$

is a non-negative monotonically increasing phase function, with a carrier frequency defined aa

$$f_1 \triangleq f_0 - \frac{h}{2T}(M-1). \qquad (8)$$

If wc now let $\{u_i\}$ be the *tilted* information *sequence*

$$u_i \triangleq (\alpha_i + (M-1))/2, \qquad u_i \in \{0,1,2,\ldots,M-1\} \qquad (9)$$

and

$$t \triangleq \tau + nT, \qquad (10)$$

then the tilted phase, $\Psi(t,u)$ can be expressed as

$$\Psi(\tau + nT, u) = 2\pi h \sum_{i=0}^{n-1} u_i + 4\pi h u_n f(\tau) + \pi h(M-1)\frac{\tau}{T} - 2\pi h(M-1) f(\tau), \quad 0 < \tau < T. \qquad (11)$$

The first term in (11) represents the state (which is from an alphabet that is expanding in size) of the waveform at time nT; the second term describes the information-bearing phase variation during the nth time period, and is independent of the state of the waveform. In that sense, the tilted phase CPM is time-invariant. The phase variations from the remaining terms in (11) keep $\Psi(\tau + nT, u) \geq 0$.

A *mod* 2π or *physical tilted phase* is now defined as

$$\tilde{\Psi}(\tau + nT, u) \triangleq mod_{2\pi}[\Psi(\tau + nT, u)], \qquad 0 \leq \tau < T, \qquad (12)$$

where $mod_\beta[\gamma]$ denotes γ modulo β; $\tilde{\Psi}(\tau + nT, u)$ is now constrained to the interval $[0, 2\pi)$.

Let V_n represent the present state, which is defined as the modulo P accumulation at time nT of the data input symbols from time O to (n -- 1)7', namely

$$V_n \triangleq mod_P \left[\sum_{i=0}^{n-1} u_i\right] \qquad (13)$$

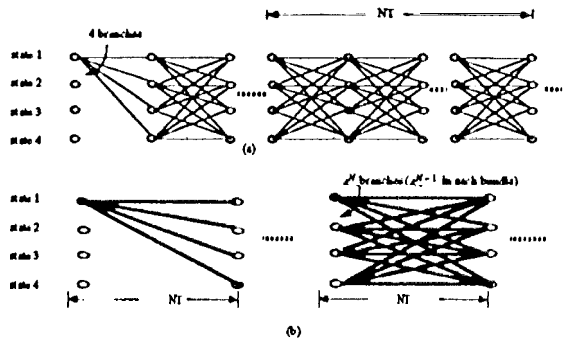

Figure 1: (a): trellis for simple CPE with M=4 (b): trellis for NCPE

where P is the integer in the denominator [1] of the definition of h in (3). In addition, wc define the vector

$$X_n \triangleq [V_n, u_n] \qquad (14)$$

to represent the present state, V_n, duc to all previous data symbols, and the present data symbol, u_n. The modulated signal over the time interval $[nT, (n+1)2')$ can be expressed as

$$s(\tau + nT, X_n) \triangleq \sqrt{\frac{2\mathcal{E}}{T}} \cos(2\pi f_1(\tau + nT) + \tilde{\Psi}(\tau, X_n) + \varphi_0), \quad 0 \leq \tau < T \qquad (15)$$

with f_1 as defined in (8).

Consequently the next state, V_{n+1}, will be represented by the present state, V_n, and the present input, u_n, i.e. $V_{n+1} = V_n + u_n$ from (13), The signal in (15) depends on the present state V_n and the present input U_n at time nT.

3 CPE, NCPE and Memory-lcss Modulator

We can now design the CPE which generates the waveform in (15) for the transition from the present state V_n in (13) to the next state, V_{n+1}, using the input u_n (see [3]). Figure l(a) shows the state trellis structure of the CPE for the case of the full response CPM with modulation index I/M, where $M = 4$. By combining N time slots together, wc can make the

[1] When $K = 1$, the smallest change in phase during the baud time T is $(2\pi/P)$ radians.

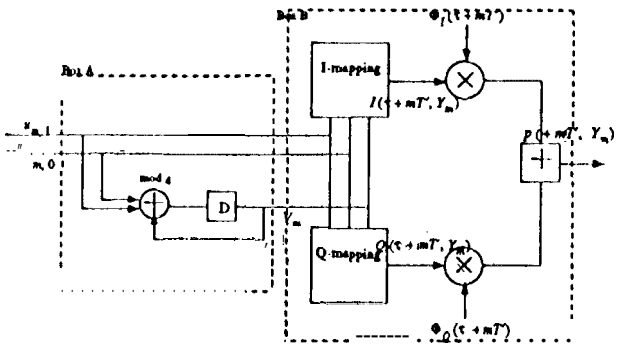

Figure 2: System configuration for uncoded 2 consecutive 4-ary full response CPFSK with parallel inputs.

state trellis structure for an arbitrary windows of NT' seconds in Figure 1 (b) for $M = 4$. This trellis structure in Figure l(b) can be implemented by the NCPE (N consecutive continuous phase encoder). There are MN branches leaving each state, which can be viewed as M bundles (which are represented by bold lines in Figure l(b)) and each bundle has MN-l branches so that each bundle represents M^{N-1} parallel transitions. Each branch specifics an N consecutive CPM signal over NT sec. Therefore, each branch in Figure 1(b) can be represented by an $(N + 1)$ dimensional vector whose elements arc from the set, {O, 1,2,3, ... M–l}. *In* this paper we concentrate on the two consecutive 4-ary CPFSK waveform i.e. N = 2, $M = 4$, and $h = 1/4$. Figure 2 shows an uncoded 4-ary CPFSK waveform generator which is composed of a 2 *consecutive continuous phase encoder* (2CPE) (Box A) and an MM (memoryless modulator) (Box B).

To denote the phase variation during two time intervals, another representation of the physical tilted phase is introduced:

$$\tilde{\Psi}_2(\tau + mT, Y_m) \triangleq \begin{cases} mod_{2\pi}\left[\frac{\pi}{2}V_m + \frac{\pi u_{m,0}}{2}\frac{\tau}{T}\right], & \text{if } 0 < \tau < T' \\ mod_{2\pi}\left[\frac{\pi}{2}(V_m + u_{m,0}) + \frac{\pi}{2}\frac{u_{m,1}}{T}(\tau - T')\right], & \text{if } T' < \tau < 2T, \end{cases} \quad (16)$$

where

$$m \triangleq \left\lfloor \frac{n}{2} \right\rfloor, \quad (17)$$

$\lfloor x \rfloor$ denotes the largest integer which is not greater than x, and

$$Y_m \triangleq (V_m, u_{m,0}, u_{m,1}), \qquad V_m, u_{m,0}, u_{m,1} \in \{O, 1,2,3\}. \quad (18)$$

The three dimensional vector, Y_m, consists of the state at time $2mT$: V_m, the input data symbol at time $2mT$: $u_{m,0}$, and the input data symbol at time $(2m + 1)T$: $u_{m,1}$. V_m *is* represented by the summation of the data symbols from time O to (2rn - 1)7'. The next state, V_{m+1}, is determined from V_m, $u_{m,0}$, and $u_{m,1}$, (i.e., $V_{m+1} = V_m + u_{m,0} + u_{m,1}$). The feedback encoder in Box A in Figure 2 generates the state transition of the physical tilted phase in (16), which is represented by the trellis in Figure l(b), where N = 2. In addition, serial data symbols, $u_{m,o}$ and $u_{m,1}$, are converted to parallel data symbols applied to the 2CPE at time $2mT$. Finally, the output waveform during time period $[2mT, 2(m + 1)7')$ is generated by the MM (memoryless modulator), and is given by

$$p(\tau + mT', Y_m) \triangleq \sqrt{\frac{2\mathcal{E}}{T}} \cos(2\pi f_1(\tau + mT') + \tilde{\Psi}_2(\tau, Y_m) + \text{PO}), \quad O < \tau < T', \quad (1.9)$$

where $p(\tau + mT', Y_m)$ denotes a modulated waveform over two time intervals and $7' = 27'$. The memoryless modulator (MM) generates the 64 different waveforms which depend on the value of Y_m. For each state (V_m), there arc 16 possible waveforms based upon the parallel input data vector $(u_{m,0}, u_{m,1})$.

For the realization of MM, it is convenient to decompose (15) into in-phase and quadrature components,

$$p(\tau + mT', Y_m) \triangleq I(\tau + mT', Y_m)\Phi_I(\tau + mT') + Q(\tau + mT', Y_m)\Phi_Q(\tau + mT') \quad (20)$$

where

$$I(\tau + mT', Y_m) \triangleq \sqrt{\mathcal{E}/T}\cos\tilde{\Psi}(\tau + mT', Y_m)$$
$$Q(\tau + mT', Y_m) \triangleq \sqrt{\mathcal{E}/T}\sin\tilde{\Psi}(\tau + mT', Y_m) \quad (21)$$

and

$$\Phi_I(\tau + mT') \triangleq \sqrt{1/2}\cos[2\pi f_1(\tau + mT') + \varphi_0]$$
$$\Phi_Q(\tau + mT') \triangleq -\sqrt{1/2}\sin[2\pi f_1(\tau + mT') + \varphi_0] \quad (22)$$

4 Set partitioning and Pre-encoder Design

It is our goal in this section to design a binary pre-encoder so that more states arc added to the states of CPE. To design a pre-encoder, it is convenient to change the CPE of Figure 2, which has feedback, into an *equivalent encoder* (see *[6])* without feedback. The equivalent encoder, shown in Figure 3(a), has two 4-ary inputs, and three 4-ary outputs which are represented by the elements of the vector Z_m:

$$Z_m \triangleq (z_{m,0}, z_{m,1}, z_{m,2}), \qquad z_{m,i} \in \{O, 1,2,3\}, \quad (23)$$

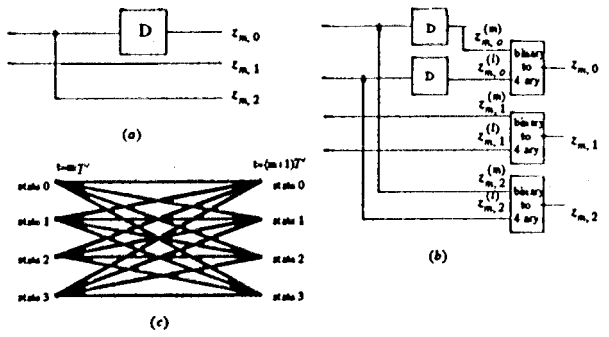

Figure 3: (a): 2CPE without a feedback (b): binary representation of 2CPE (c): trellis structure of 2CPE

where

$$z_{m,0} \triangleq V_m$$
$$z_{m,1} \triangleq mod_4[-u_{m,1}]$$
$$z_{m,2} \triangleq mod_4[V_m + u_{m,0} + u_{m,1}], \qquad (24)$$

where $V_m, u_{m,0}$, and $u_{m,1}$ *is* defined in (18) as elements of Y_m. There is a one to one correspondence between Z_m and Y_m; therefore, an output signal in the time period [mZ", $(m + 1)T'$) can be decided by the vector Z_m by the relations shown in (16), (19), and (24). Precise] y, $z_{m,0}$ of Z_m denotes the state of 2CPE at time mT', $z_{m,2}$ denotes the next state at time (m+ $1)T'$, and $z_{m,1}$ denotes a branch in the parallel transition of four branches (which is represented by a bold line in Figure 3(c) where each bold line represents four branches). This 2CPE is changed into a binary encoder and binary-to-4-ary converters as shown in Figure 3(b).

10 partition the set of 2CPE waveforms in *(19),* the ***squared*** signal space distance should be calculated. Anderson [7] has derived the squared signal space distance, d_n^2, between two signals, $s^{(1)}(t)$ and $s^{(2)}(t)$, in (15) during the time interval $[nT, (71 + 1)?')$ when $f_1 >> 1/T$, namely

$$d_n^2 \,(S(l), S(2)) = \begin{cases} 2\left(1 - \frac{\sin \Delta\Psi_{n+1} - \sin \Delta\Psi_n}{\Delta\Psi_{n+1} - \Delta\Psi_n}\right), & \text{if } \Delta\Psi_{n+1} \neq \Delta\Psi_n \\ 2(1 - \cos \Delta\Psi_n), & \text{otherwise,} \end{cases} \qquad (25)$$

where $\Delta\Psi_n$ denotes the phase difference of two signals $s^{(1)}$ and $s^{(2)}$, at time nT. The squared distance of the signals during *two* time intervals, is expressed by the sum of the squared distances in (25) for each time interval. The squared distance of each time interval is derived as a function of $\Delta Y_m = Y_m^{1)} - Y_m^{(2)}$, where $Y_m^{(1)}$ and $Y_m^{(2)}$ arc vectors which represent two possible

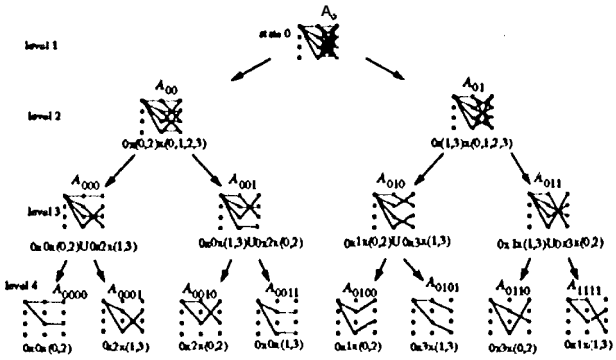

Figure 4: Set partitioning of 2 consecutive 4-ary CPFSK signals

signals $p^{(1)}(\tau - t\ ml'")$ and $p^{(2)}(\tau + mT')$. Therefore, the squared distance during two time intervals is a function of the difference vector, ΔY_m, of two vectors which represent the two candidate signals,

$$d_m^2(\Delta Y_m) \triangleq d_{m1}^2(\Delta Y_m) + d_{m2}^2(\Delta Y_m) \qquad (26)$$

where

$$d_{m1}^2(\Delta Y_m) = \begin{cases} 2\left(1 - \frac{\sin \frac{\pi}{2}(\Delta V_m + \Delta u_{m,0}) - \sin \frac{\pi}{2} \Delta V_m}{\frac{\pi}{2} \Delta u_{m,0}}\right), \\ \quad \text{if } \Delta u_{m,0} \neq 0 \\ 2(1 - \cos \frac{\pi}{2} \Delta V_{m,0}), \\ \quad \text{if } \Delta u_{m,0} = 0 \end{cases} \qquad (27)$$

and

$$d_{m2}^2(\Delta Y_m) = \begin{cases} 2\left(1 + \frac{\sin \frac{\pi}{2}(\Delta V_m + \Delta u_{m,0} + \Delta u_{m,1}) - \sin \frac{\pi}{2}(\Delta V_m + \Delta u_{m,0})}{\frac{\pi}{2} \Delta u_{m,1}}\right), \\ \quad \text{if } \Delta u_{m,1} \neq 0 \\ 2(1 - \cos \frac{\pi}{2} \Delta(V_m + u_{m,0}), \\ \quad \text{if } \Delta u_{m,1} = 0 \end{cases} \qquad (28)$$

where $\Delta Y_m = (\Delta V_m, \Delta u_{m,0}, \Delta u_{m,1})$. Also, d_{m1} and d_{m2} represent the signal space distance during *[2mT,* **(2rn + 1)7')** and $[(2m + 1)T, 2(rn + 1)T)$, respectively.

Figure 4 shows the set partitioning of signals which diverge from the same state of 2CPE. For convenience in representing the waveforms in (19), each of the 16 candidate signals is represented by onc path from a state at mT' to a state at (m + 1)2'" through an intermediate state at $(2rn + 1)T$. In level 1, A_i represents the 16 different signals which diverge from each state i $\in$ {O, 1, 2, 3} (Figure 4 is an example when i = O). The signals in A_i are successively partitioned into 2, 4 and 8 subsets of size 8, 4 and 2 respectively, which have progressively larger minimum *intradistances* (which is

the distance between two signals in the same subset). The partition is made so that the minimum squared intradistance within each partitioned signal subset is maximum and the sets of squared intradistances for the partitioned signal subsets in each level are equal. In Figure 4, for example, the signal set resulting from each partition is denoted by the Cartesian product (e.g. O x (O, 2) x (O, 1,2,3) in Ao_o denotes the set {(0,0,0),(0,0,1) (O, 0,2),(0,0,3),(0,2, O),(O,2,l),(O,2,2), (0,2,3))). Each vector represents Z_m as defined in (23) and (24). The squared intradistance set for the signals in A. is $\{0.727\mathcal{E}, 1.454\mathcal{E}, 2.0\mathcal{E},$ 2.7278, 4. $0\mathcal{E}$, 4.4248, 4.8496, 5.2738, 5.6978, $6.0\mathcal{E}$, 7.273 S}, based on the calculation of (26) with (27) and (28). We separate Ao into two subsets in order to exclude the squared intradistance values: $0.727\mathcal{E}$ and $1.454\mathcal{E}$, by separating the signals with these squared distances, into different subsets. In level 2 the squared intradistance set is $\{2.0\mathcal{E},$ 2.727&, 4. $0\mathcal{E}$, 4.424&, 5.697&, $6.0\mathcal{E}\}$, where the minimum squared intradistance is $2.0\mathcal{E}$. We partition the level 2 sets by separating signals whose squared distance is $2.0\mathcal{E}$ or 2.727&. The resulting signals in level 3 have the squared distances $\{4.0\mathcal{E}, 5.697\mathcal{E}, 6.0\mathcal{E}\}$ where the minimum squared intradistance is $4.0\mathcal{E}$. The last partitions eliminate the squared distances $4.0\mathcal{E}$ and 5.692&, so that the minimum squared intradistance of level 4 subsets is $6.0\mathcal{E}$.

Figure 6(a) shows the trellis structure for the pre-encoder state transition. We have assigned the level 3 subsets to parallel transitions and the level 2 subsets to the trellis branches leaving from the same state. The pre-encoder shown in Box A of Figure 6(b), is designed to implement the trellis structure shown in Figure 6(a). The least significant bit, $z_{m,1}^{(l)}$, of $z_{m,1}$ determines the state of the encoder as well as the subset from the level 2 subsets in Figure 4. The least significant bits (i.e. each $z_{m,1}^{(l)}$) of the elements in Aoo arc O and the least significant bits (i.e. each $z_{m,1}^{(l)}$) of the elements in Ail are 1. Therefore we have made a connection between the output of the delay element and $z_{m,1}^{(l)}$ and realized the pre-encoder with a systematic *feedback encoder* (see *[6]).* In order to find the encoder which has the largest *free distance* d_{free}^2, a computer search was used for all the possible connections between the binary summer, represented by $\oplus$, and the three binary input lines $(z_{m,1}^{(m)}, z_{m,2}^{(l)}, z_{m,2})$ and the feedback line $(z_{m,1}^{(l)})$. The best encoder (Figure 6(b)) we found shows that $z_{m,2}^{(l)} \oplus z_{m,1}^{(m)} \oplus z_{m,1}^{(l)}$ decides the next state of the prc-encoder, and the level 3 subsets in Figure 4 show that $z_{m,2}^{(l)} \oplus z_{m,1}^{(m)} \oplus z_{m,1}^{(l)}$ determines the subset to which Z_m belongs. The path corresponding to d_{free}^2 is the path denoted by the encoder output (0,2,1) and (1,0,0) shown in Figure 6(c). Wc found that d_{free}^2 = 6.424413$. The power gain over the uncodcd 4-ary CPFSK is 5.2 dB, and the power gain over the uncodcd 2-ary CPFSK is 3.3 dB where normalizing with respect to the bit energy, and where we assumed the use of *Viterbi decoding* (see *[5]).*

Table 1: Summary of d_{free}^2 and Power Gain

number of states	d_{free}^2	Gain over Uncoded 4CPFSK	Gain over Uncoded 2CPFSK
2	$6.424413\mathcal{E}$	5.2047 dB	3.3071 dB
4	$8.000000\mathcal{E}$	6.1573 dB	4.2597 dB
8	$8.907042\mathcal{E}$	6.6237 dB	4.7261 dB
16	$10.848826\mathcal{E}$	7.48023 dB	5.5826 dB

Table 2: Bandwidth Comparison.

New Coded 4CPFSK	Uncoded 4CPFSK	Uncoded 2CPFS
1	0.75	1.5

Figure 7 shows the 4 state case. The level 4 subsets were assigned to parallel transitions in tbc pre-encoder in Box A. Figures 8 and 9 show the 8-state and 16-state cases respectively. Table 1 summarizes the d_{free}^2 and power gain that is achieved with these structures. Table 2 shows the bandwidth comparison. Because of the use of 3/4 rate coding, our system requires more bandwidth than the uncodcd 4-ary CPFSK waveform to get the same data transmission rate.

By assuming high SNR, asymptotic bit error probability has been evaluated for the two state trellis coded two-consecutive 4-ary CPFSK with a coding rate of 3/4, and the uncodcd 4-ary CPFSK based on the d_{free}^2 results in Table 1 (see [8]):

$$P_b(e) \approx \frac{N_e(d_{free})}{N_b(frame)} Q\left(\sqrt{\frac{d_{free}^2}{2N_0}}\right), \qquad (29)$$

where Q(.) is the Gaussian integral function, $N_e(d_{free})$ is the number of erroneous bits in the path corresponding to d_{free}, and $N_b(frame)$ is the number of transmitting bits in one signal frame. In Figure 5, we present the simulation results and asymptotic values of bit error probability for the uncoded case and the 2-state coded case. Based on the simulation results, e.g., at P_b = lo-^{4} there is an improvement of 4.3 dB in bit SNR. Based on the asymptotic analysis result, the improvement is about $5.2dB$ at high bit SNR (in Figure 5 and 'I'able 1).

5 Conclusion and Discussion

In Rcferenccs [4] and [9], several encoders for 4-ary CPFSK systems whose rate is 1/2 were designed. These have power gains from 3 d B to 7.63 dB over the

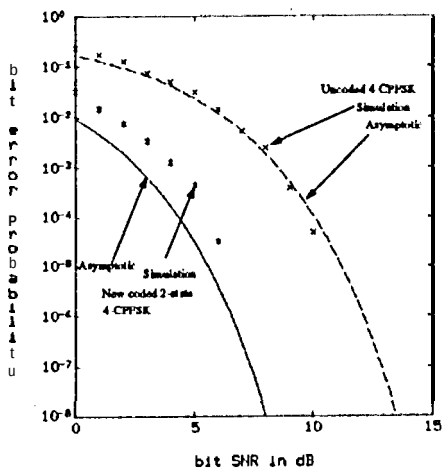

Figure 5: Analytical and simulation results for bit error probability of two-state trellis coded two-consecutive 4-CPFSK with a coding rate of 3/4 and uncoded 4-CPFSK

uncoded system depending on the number of states. However, this system requires twice the bandwidth for the same transmission rate . By combining the time slots together, wc can design higher rate encoders and have more flexibility for assigning the signals to the trellis branches as shown by the work in [1] and [2].

Our results here show that wc can obtain a significant power gain *(5.20* dB to 7.48 dB) at the expense of a reduction in bandwidth efficiency for the same data transmission rate over the uncoded case, We have designed pre-encoders with a coding rate of 3/4 which have better bandwidth efficiency than the N=1 coded 4-ary CPFSK system with a coding rate of 1/2 because of the higher coding rate. However, the trade offs for these advantages arc more complexity and decoding delay.

Memoryless mapping could be designed to assign sets of 64 signals to the output of the combined encoder. This can be separated into two separate memoryless mappings so that each memoryless mapper assigns output signals to each time slot. Each branch of trellis needs two time slots, so there is an additional but nominal time delay to decode the received signal sequence.

References

[1] Steven S. Pietrobon, Robert H. Deng, Alain Lafanechere, Gottfried Ungerboeck, and Daniel J. Costello. Jr. "Coded Multidimensional Phase Modulation." *IEEE Transaction on* **Information Theory,** VOL 36, pp. 63-89, JAN. 1990.

[2] Lee-Fang Wci. "Trellis-Coded Modulation with Multidimensional Constellations." *IEEE Transaction on Information Theory,* VOL 33, pp. 483-501, JUL. 1987.

[3] Bixio Rimoldi. "A Decomposition Approach to CPM." *IEEE Transaction on information Theory,* VOL 34, pp. 260-270, MARCH 1988.

[4] Bixio Rimoldi. "Design of Coded CPFSK Modulation Systems for Bandwidth and Energy Efficiency." *IEEE Transaction on Communications,* VOI, 37, pp. 897-905, SEP. 1989.

[5] G .D.Forney."The Viterbi Algorithm ." ***Proceedings of the IEEE,*** VOL 61, pp. 433--441, MARCH 1973.

[6] G .D.Forney. "The Convolutional Codes I." *IEEE Transaction on Information Theory,* **VOL 16,** pp. 720-738, NOV 1970.

[7] John B Anderson and Desmond P. Taylor. "A Bandwidth-Efficient Class of Signal-Space Codes." *IEEE* **Transaction *on Information Theory,*** VOL 24, pp. 703-712, NOV. 1978.

[8] Gottfried Ungerboeck. "Channel Coding with Multilevel/Pha~c signals." IEEE *Transaction on Information Theory,* VOL 28, pp. 55-66, JAN. 1982.

[9] S. V. Pizzi. "Convolutional Coding Combined with Continuous Phase Modulation." *IEEE Transaction on Communications,* VOL 33, pp. 20-29, JAN. 1985.

Acknowledgment

The research described in this paper was carried out by the Jet Propulsion Laboratory, California Institute of Technology, and the University of Southern California under a contract with the National Aeronautics and Space Administration.

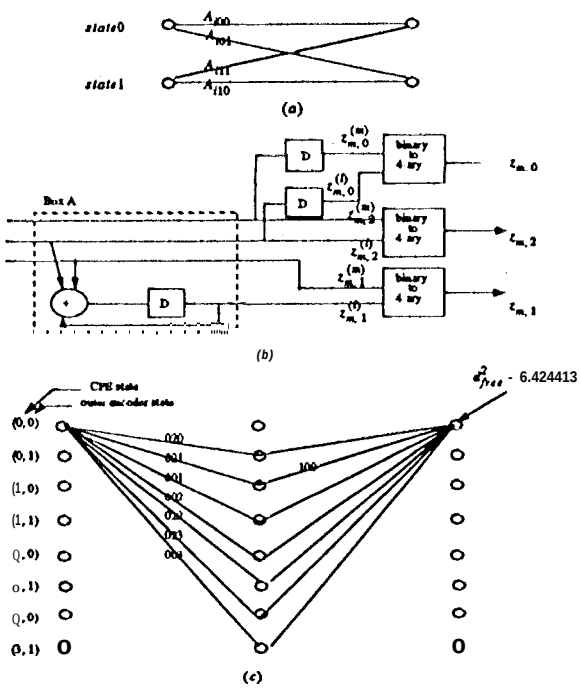

Figure 6: (a): 2 states pm-encoder trellis structure (b): combined encoder (c): path for d^2_{free}

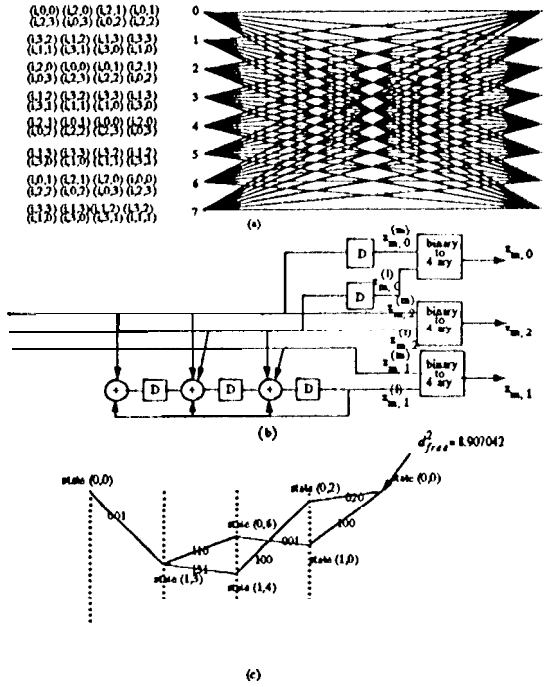

Figure 8: (a): 8 states pre-encoder trellis structure (b): combined encoder (c): path for d^2_{free}

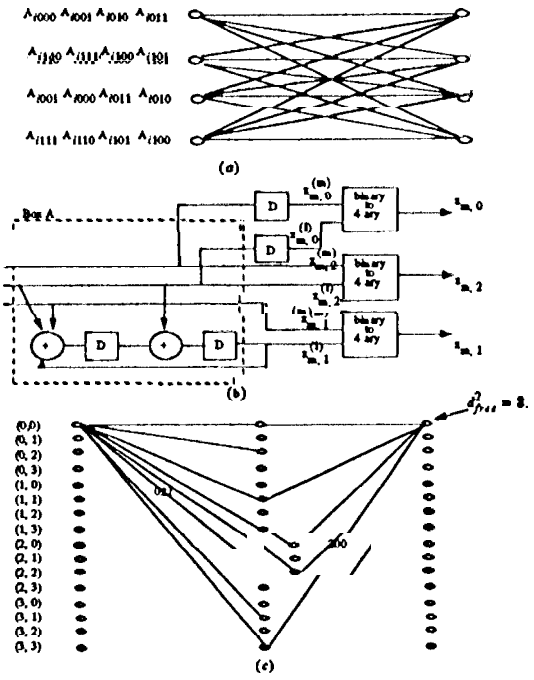

Figure 7: (a): 4 states pre-encoder trellis structure (b): combined encoder (c): path for d^2_{free}

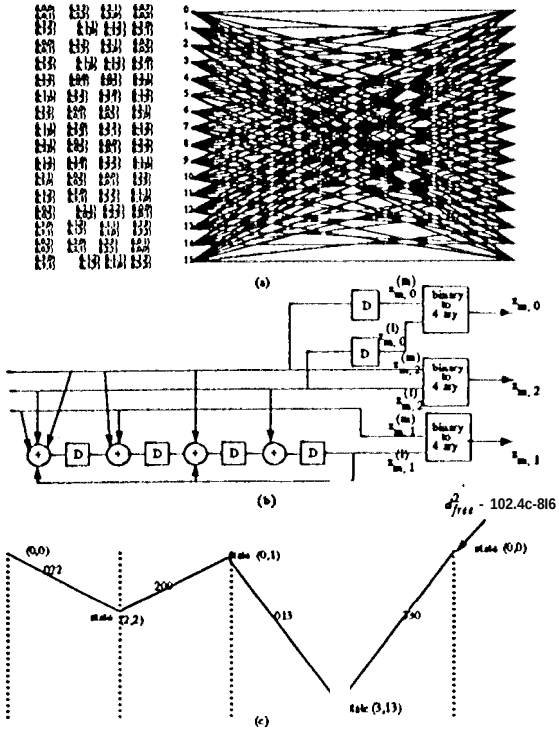

Figure 9: (a): 16 states pre-encoder trellis structure (b): combined encoder (c): path for d^2_{free}